A&A 365, 341–346 (2001)
DOI: 10.1051/0004-6361:20000187


Astronomy & Astrophysics

# Using the COBE/DMR data as a test-bed for normality assessments

N. Aghanim[1], O. Forni[1], and F. R. Bouchet[2]

[1] IAS-CNRS, Université Paris Sud, Bâtiment 121, 91405 Orsay Cedex, France
[2] IAP-CNRS, 98 bis Boulevard Arago, 75014 Paris, France

Received 10 May 2000 / Accepted 28 September 2000

**Abstract.** A very important property of a statistical distribution is to know whether it obeys Gaussian statistics or not. On the one hand, it is of paramount importance in the context of CMB anisotropy studies, since deviations from a Gaussian distribution could indicate the presence of uncorrected measurement systematics, of remaining fluctuations contributed by foregrounds, of deviations from the simplest models of inflation or of topological defects. On the other hand, looking for a non-Gaussian signal is a very ill-defined task and performances of various assessment methods may differ widely when applied in different contexts. In previous studies, we introduced a sensitive wavelet-based method which we apply here to the COBE/DMR data set, already extensively studied, using different approaches. This provides an objective way to compare methods. It turns out that our multi-scale wavelet decomposition is a sensitive method. Yet, we show that the results are rather sensitive to the choice of both the decomposition scheme and the wavelet basis. We find that the detection of the non-Gaussian signature is "marginal" with a probability of at most 99%.

**Key words.** Cosmology: cosmic microwave background – methods: data analysis, statistical

## 1. Introduction

The COBE-DMR data (Smoot et al. 1992) give the distribution of temperature anisotropies of the Cosmic Microwave Background (CMB) on most of the sky with a resolution of about 10°. This data set was the first to put constraints on the spectral index and the amplitude of the initial power spectrum (Fixsen et al. 1996). Further analyses of the CMB anisotropies should also give hints on the dominant mechanism which generates the initial density perturbation. As a matter of fact, the simplest inflation models generally predict a normal (Gaussian) distribution of the perturbations whereas the topological defects generate a non-Gaussian distribution.

Many studies have aimed at characterising the statistical properties of the COBE/DMR data (Amendola 1996; Kogut et al. 1996; Ferreira et al. 1998; Heavens 1998; Pando et al. 1998b; Schmalzing & Gorski 1998; Bromley & Tegmark 1999; Magueijo 2000; Mukherjee et al. 2000). These investigations have relied on various statistical indicators both in the real space (e.g. high order moments of the temperature distribution, Minkowski functionals, genus analysis, ...) and in the dual, Fourier or wavelet transformed, space (e.g. $N$-point correlation functions, cumulants and moments of coefficients, ...). The COBE/DMR temperature fluctuations have long been considered Gaussian distributed. However more recently, their statistical nature has been debated, as some of the groups mentioned above found a non-Gaussian signature in the COBE/DMR four year maps.

Regardless of the implications of such a signature, we use the COBE/DMR data as the only available test-bench for applying, on real maps, a method proposed in Aghanim & Forni (1999) and Forni & Aghanim (1999), geared at detecting non-Gaussian features. This method is based on the statistical analysis of the wavelet coefficients obtained after a multi-scale decomposition of the signal. In fact, the non-Gaussian signatures are enhanced in the wavelet space, which makes an analysis in this space more sensitive to the statistical signatures. In this context, the major differences between the methods based on wavelets come from the choices of the decomposition scheme and the wavelet basis. We briefly describe these choices and the method in Sect. 2. We present our results and discuss them in respectively Sects. 3 and 4. Finally, we give our main conclusions in Sect. 4.

## 2. Data and analysis method

The COBE/DMR four year data was "cleaned" from the contribution of the galactic foreground emissions using two methods. One is based on a combination technique

*Send offprint requests to*: N. Aghanim,
e-mail: aghanim@ias.fr

(linear combination of the DMR maps) and results on what we refer to as the DCMB maps. The second technique is based on the subtraction of the galaxy contribution and it gives the DSMB maps.

Wavelet analyses were shown to be very useful tools to detect non-Gaussian signatures on simulated CMB maps (Aghanim & Forni 1999; Hobson et al. 1999). They were applied on the COBE/DMR maps by Pando et al. (1998b) and more recently in an exhaustive study by Mukherjee et al. (2000). In this paper, we re-analyse both sets of COBE/DMR data (DCMB and DSMB) to study their statistical nature (Gaussian or non-Gaussian). In order for our conclusions to be the most independent possible of the cleaning method, we have analysed the less contaminated regions of the COBE/DMR sky namely: the northern and the southern poles. These regions are associated respectively with the faces #1 and #6 of the so-called COBE cube on which the data were projected.

Based on the method proposed in Forni & Aghanim (1999), we decompose the signal on the wavelet basis and compute the kurtosis which is the fourth order moment of the wavelet coefficient distribution. We thus derive the excess of kurtosis, that is the deviation from the predicted value in a Gaussian distribution. The values obtained are compared with the excesses of kurtosis calculated using 2000 Gaussian realisations of the COBE/DMR maps. These Gaussian realisations have the same power spectra as the COBE/DMR maps with truly random phases, everything else (pixel size, coverage) being kept the same. Any statistical difference between the excess of kurtosis measured on COBE/DMR and those measured on the associated Gaussian realisations should thus be associated with the non-Gaussian character of the data.

The wavelet analysis consists in hierarchically decomposing an input signal into a series of successively lower resolution "reference" signals and their associated "detail" signals (Mallat 1989). At each decomposition level, $L$, the reference signal has a resolution reduced by a factor of $2^L$ with respect to the input signal. Due to the orthogonality properties of the basis, a function can be completely characterised by the wavelet basis and the wavelet coefficients of the decomposition. We test the detection of non-gaussianity against the wavelet basis in the "dyadic" decomposition scheme. We will compare our results with a study based on an alternative decomposition scheme: the "pyramidal" decomposition (Mukherjee et al. 2000). The dyadic decomposition is a transform in which, at each level $L$, only the reference signal (low-pass part of the signal) is decomposed. At each decomposition level, the analysis is applied in both directions and the total number of sub-bands after $L$ levels of decomposition is $3L + 1$. The pyramidal decomposition is similar to the previous decomposition in the sense that only the reference sub-band is decomposed at each level. However, it is performed here separately in the two directions of the image. The total number of sub-bands after $L$ levels of decomposition is then $(L + 1)^2$.

The choice of the wavelet basis is critical to test for non-gaussianity. We expect that the non-Gaussian features are due to point sources or sharp gradients in the signal. The detection of non-gaussianity is based on the search of these gradients. We therefore choose to use anti-symmetric wavelets which are proportional to, or almost proportional to, a first derivative operator and thus particularly sensitive to gradients. In practice, we choose the 6/10 tap filter (filter #3) of Villasenor et al. (1995) mainly used in data compression. It has, in fact, a very good impulse response and a low shift variance which better preserve the amplitude and the location of the details. We have also used the commonly-used Haar wavelet which is also an anti-symmetric function.

In the dyadic wavelet decomposition and using the anti-symmetric wavelet basis, we can discriminate between the coefficients associated with vertical, horizontal and diagonal gradients. They are analogous to the partial derivatives, respectively $\partial/\partial x$, $\partial/\partial y$ and $\partial^2/\partial x \partial y$ of the signal.

The maps we analyse have $32 \times 32$ pixels, with a pixel of $2.8^\circ$ aside. Due to this reduced number, we restrict to a three level decomposition. The three decomposition scales (hereafter I, II and III) correspond respectively to an angular scale $\theta = 5.6^\circ$ (that is a multipole order $\ell = 35.7$), $\theta = 11.2^\circ$ ($\ell = 17.8$), and $\theta = 22.4^\circ$ ($\ell = 8.9$).

## 3. Results

### 3.1. North galactic pole

We test for the detection of a non-Gaussian signature in the COBE/DMR, DCMB map, of the north galactic pole against 2000 Gaussian realisations of this map. First using the Haar wavelet basis in a three level decomposition, we compute the excesses of kurtosis of the coefficients associated with the details for the COBE map ($k^1_{\rm COBE}$, see Table 1), and the Gaussian realisations. We give, in this case, the mean excess of kurtosis $\overline{k}$ and the standard deviations $\sigma_-$ and $\sigma_+$ with respect to this mean for the quantities that are respectively smaller and larger than $\overline{k}$. Finally, we compare the obtained results and quantify the probability $P$ that the measured excess of kurtosis on the COBE map ($k^1_{\rm COBE}$) indicates a non-Gaussian process. This probability is computed by integrating the excess of kurtosis distribution for the Gaussian realisations, one example of which is shown in Fig. 1. It ranges between about 50 and 99% depending on the decomposition scale and on the type of details we study. We note that the non-Gaussian signature is detected at all scales with at least a probability larger than 68%. However, the most significant detections at about the 98 and 99% confidence levels are obtained respectively at the second and third scales where the beam and noise effects are expected to be less dominant. In the case of the Villasenor et al. wavelet basis, the probability of detecting a non-Gaussian signature in the DCMB COBE/DMR #1 map lies between about 67 and 98% (see Table 2). Again this detection is made at all scales.

**Table 1.** For the north galactic pole and the Haar wavelet basis, the first column represents the mean excess of kurtosis computed with the wavelet coefficients over 2000 Gaussian realisations of the COBE/DMR #1 map (DCMB). $\sigma_-$ and $\sigma_+$ are the standard deviations with respect to the mean of the kurtosis distribution. The fourth column represents the excess of kurtosis computed on the COBE/DMR map and the last column gives the probability, computed with the corresponding distribution, for the excess of kurtosis $k^1_{\rm COBE}$ to indicate a non-Gaussian signal

| Scale I | $\overline{k}$ | $\sigma_-$ | $\sigma_+$ | $k^1_{\rm COBE}$ | $P$ |
|---|---|---|---|---|---|
| $\partial/\partial x$ | 0.005 | 0.26 | 0.34 | 0.15 | 72.4% |
| $\partial/\partial y$ | −0.006 | 0.27 | 0.36 | −0.22 | 77.6% |
| $\partial^2/\partial x\partial y$ | 0.01 | 0.26 | 0.35 | −0.30 | 87.8% |
| Scale II | | | | | |
| $\partial/\partial x$ | 0.03 | 0.50 | 0.84 | −0.51 | 84.6% |
| $\partial/\partial y$ | −0.002 | 0.48 | 0.79 | −0.35 | 76% |
| $\partial^2/\partial x\partial y$ | −0.02 | 0.46 | 0.76 | 1.37 | 97.6% |
| Scale III | | | | | |
| $\partial/\partial x$ | −0.03 | 1.01 | 1.88 | −0.30 | 50.2% |
| $\partial/\partial y$ | 0.02 | 0.99 | 1.81 | −1.85 | 98.7% |
| $\partial^2/\partial x\partial y$ | 0.02 | 1.04 | 1.95 | 1.08 | 81.6% |

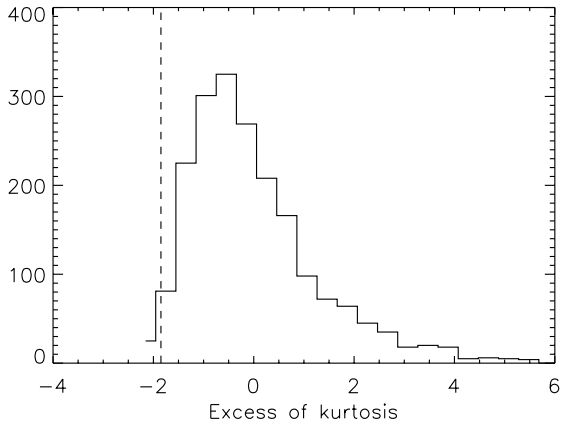


**Fig. 1.** For the north galactic pole of the COBE/DMR #1 map (DCMB) and the Haar wavelet basis, we show the distribution of the excesses of kurtosis computed with the wavelet coefficients ($\partial/\partial\, y$) at the third decompostion scale for 2000 Gaussian realisations. The vertical dashed line represents the excess of kurtosis measured on the COBE map with a probability of 98.7% (cf. line 8, Table 1)

We perform the same analysis using the two wavelet bases on the COBE map obtained with the second subtraction technique (DSMB maps). In Table 5, we give the probability for the excess of kurtosis, measured on the COBE/DMR map, to be associated with the detection of a non-Gaussian signal. We note again that the probabilities indicate a non-Gaussian process at all scales. The Haar basis seems however to give smaller (less discriminating) values than the Villasenor et al. basis.

**Table 2.** Same as Table 1, for the the Villasenor et al. wavelet basis

| Scale I | $\overline{k}$ | $\sigma_-$ | $\sigma_+$ | $k^1_{\rm COBE}$ | $P$ |
|---|---|---|---|---|---|
| $\partial/\partial x$ | 0.004 | 0.26 | 0.30 | 0.75 | 98% |
| $\partial/\partial y$ | 0.01 | 0.27 | 0.39 | 0.75 | 97.7% |
| $\partial^2/\partial x\partial y$ | 0.007 | 0.27 | 0.36 | −0.18 | 73.3% |
| Scale II | | | | | |
| $\partial/\partial x$ | 0.01 | 0.48 | 0.78 | 0.59 | 87.5% |
| $\partial/\partial y$ | 0.03 | 0.50 | 0.87 | −0.41 | 79.3% |
| $\partial^2/\partial x\partial y$ | 0.04 | 0.50 | 0.83 | 0.79 | 89.9% |
| Scale III | | | | | |
| $\partial/\partial x$ | −0.01 | 1.0 | 1.79 | −0.77 | 66.8% |
| $\partial/\partial y$ | 0.02 | 1.02 | 1.83 | −1.17 | 86.3% |
| $\partial^2/\partial x\partial y$ | 0.005 | 0.99 | 1.83 | −1.59 | 95.6% |

**Table 3.** For the south galactic pole and the Haar wavelet basis, the first column represents the mean excess of kurtosis computed with the wavelet coefficients for 2000 Gaussian realisations of the COBE/DMR #6 map (DCMB). $\sigma_-$ and $\sigma_+$ are the standard deviations with respect to the mean of the kurtosis distribution. The fourth column represents the excess of kurtosis computed on the COBE/DMR map and the last column gives the probability, computed with the corresponding distribution, for the excess of kurtosis $k^6_{\rm COBE}$ to be associated with a non-Gaussian signal

| Scale I | $\overline{k}$ | $\sigma_-$ | $\sigma_+$ | $k^6_{\rm COBE}$ | $P$ |
|---|---|---|---|---|---|
| $\partial/\partial x$ | 0.006 | 0.26 | 0.35 | −0.28 | 85.7% |
| $\partial/\partial y$ | −0.01 | 0.26 | 0.36 | −0.21 | 75.8% |
| $\partial^2/\partial x\partial y$ | 0.02 | 0.27 | 0.35 | −0.28 | 85.7% |
| Scale II | | | | | |
| $\partial/\partial x$ | 0.03 | 0.50 | 0.82 | −0.56 | 87.6% |
| $\partial/\partial y$ | 0.003 | 0.49 | 0.80 | 0.59 | 87.7% |
| $\partial^2/\partial x\partial y$ | −0.03 | 0.46 | 0.75 | −0.62 | 91.5% |
| Scale III | | | | | |
| $\partial/\partial x$ | −0.03 | 1.01 | 1.89 | −0.68 | 67.5% |
| $\partial/\partial y$ | 0.007 | 0.99 | 1.81 | −1.27 | 90.3% |
| $\partial^2/\partial x\partial y$ | 0.005 | 1.03 | 1.93 | 0.40 | 52.9% |

### *3.2. South galactic pole*

Using the power spectrum of the COBE/DMR #6 map (DCMB) of the south galactic pole, we again simulate 2000 Gaussian realisations of this map. We perform the wavelet decomposition using the Haar and the Villasenor et al. bases, and analyse the statistical properties of each type of details. As for the north pole, we compute the excess of kurtosis in the COBE/DMR map ($k^6_{\rm COBE}$) and the probability, $P$, that it belongs to the distribution of the excesses of kurtosis of the Gaussian realisations. The latter is characterised by its mean $\overline{k}$ and standard deviations $\sigma_-$ and $\sigma_+$ of respectively smaller and larger values with respect to the mean. The results are summarized in Tables 3 and 4.

**Table 4.** Same as Table 3 for the Villasenor et al. wavelet basis

| Scale I | $\overline{k}$ | $\sigma_-$ | $\sigma_+$ | $k^6_{\rm COBE}$ | $P$ |
|---|---|---|---|---|---|
| $\partial/\partial x$ | 0.006 | 0.27 | 0.35 | −0.003 | 48.6% |
| $\partial/\partial y$ | 0.01 | 0.26 | 0.38 | 0.33 | 86.2% |
| $\partial^2/\partial x\partial y$ | 0.006 | 0.27 | 0.36 | 0.11 | 68.7% |
| Scale II | | | | | |
| $\partial/\partial x$ | 0.01 | 0.48 | 0.78 | −0.55 | 86.4% |
| $\partial/\partial y$ | 0.03 | 0.50 | 0.90 | 0.10 | 62.8% |
| $\partial^2/\partial x\partial y$ | 0.04 | 0.50 | 0.82 | 0.61 | 86.9% |
| Scale III | | | | | |
| $\partial/\partial x$ | −0.01 | 0.99 | 1.81 | −0.21 | 46.9% |
| $\partial/\partial y$ | 0.04 | 1.02 | 1.89 | −1.26 | 87.5% |
| $\partial^2/\partial x\partial y$ | 0.002 | 1.0 | 1.81 | 0.45 | 73.3% |

At first sight, these results suggest that the southern hemisphere distribution is more Gaussian than its northern hemisphere counterpart. As a matter of fact, the probability that the excess of kurtosis $k^6_{\rm COBE}$ measured on the COBE DCMB map indicates a non-Gaussian process lies between 53 and 92% for the Haar wavelet basis and between 47 and 87% for the Villasenor et al. wavelet. At all scales, we measure a probability larger than 68% for at least one type of details. However, these values are always smaller than those obtained for the northern hemisphere.

When we analyse the DSMB map of the southern hemisphere (Table 5), we note the same behaviour: the non-Gaussian signature is weaker in the south than in the north. The probabilities lie between 44 and 87% for the Haar wavelet basis, and between 45 and 98% for the Villasenor et al. basis. The highest probabilities, in this case, are obtained at the second decomposition scale.

### 3.3. Scale-scale correlation spectra

Another method to detect a non-Gaussian signature consists in using the scale-scale correlations as proposed by Pando et al.(1998a), Pando et al. (1998b) and Mukherjee et al. (2000). The correlations between structures at adjacent decomposition scales are quantified. They can be computed using the expression given in Mukherjee et al. (2000):

$$C_{j_1,j_2} = \frac{2^{k_1+k_2}\sum_{l_1=0}^{2^{k_1}-1}\sum_{l_2=0}^{2^{k_2}-1} < b^2_{j_1,j_2,\frac{l_1}{2},\frac{l_2}{2}} b^2_{k_1,k_2,l_1,l_2} >}{\sum_{l_1=0}^{2^{k_1}-1}\sum_{l_2=0}^{2^{k_2}-1} b^2_{j_1,j_2,\frac{l_1}{2},\frac{l_2}{2}} \sum_{l_1=0}^{2^{k_1}-1}\sum_{l_2=0}^{2^{k_2}-1} b^2_{k_1,k_2,l_1,l_2}}. \quad (1)$$

In this expression, the $b_{j_1,j_2,l_1,l_2}$ represent the coefficients in the wavelet decomposition. $C_{j_1,j_2}$ gives the correlation factor between the coefficients in the domain $(j_1, j_2)$ and its adjacent scale $(k_1, k_2)$, where $k_1 = j_1 + 1$ and $k_2 = j_2 + 1$, for a Gaussian signal $C_{j_1,j_2} = 1$. In order to assess the gain brought by this further step of analysis, we proceed as previously. We first compute the scale-scale correlation coefficients for our 2000 Gaussian realisations of the COBE/DMR maps after decomposing them on three scales with the Haar and Villasenor et al. bases. We then compute the scale-scale correlations for the "real" COBE maps and finally compute the probability that the measured numbers indicate a non-Gaussian signature by using the distribution of correlations for the Gaussian maps.

The results are summarized in Table 6. They basically agree with those obtained by Mukherjee et al. (2000) when the comparison can be made, that is for our diagonal details. The probabilities, for the correlations between scales I and II in the north galactic pole, lie between 64 and 76%, with the Haar basis, and between 62 and 99% with the Villasenor et al. basis. When we correlate scales II and III, we find a probability of 69 to 96%, with Haar; whereas it is of 61 to 88% with the Villasenor et al. basis. In the south galactic pole, the probability for the correlation coefficients between scales I and II to be associated with a non-Gaussian signal ranges between 60 and 94% with the Haar basis, and between 63 and 98% with the Villasenor et al. basis. Correlating scale II and scale III, the probabilities are between 44 and 87% with Haar and between 50 and 97% with Villasenor et al. The results obtained with the correlation coefficients agree with the direct analysis of the wavelet coefficients. However, they seem to give larger non-Gaussian signatures for the south pole than the direct analysis.

## 4. Discussion and conclusions

At each decomposition scale, we detected a non-Gaussian signature using three different criteria related to the horizontal, vertical and diagonal details of the image. We tested and compared the sensitivity to non-Gaussian features of the south and north pole maps obtained after subtracting the galaxy with two techniques. We thus analysed this four map set with two wavelet bases used in a three level dyadic decomposition. All the results are summarized in Tables 1–5.

This rather exhaustive study leads to two main conclusions. One is that the analysis of the COBE maps is rather sensitive to the choice of the wavelet basis when the same decomposition scheme is used. The second conclusion is that the non-Gaussian signature is detected with a probability of 99%. At the first and second decomposition scales, the high probalities are very likely associated with some instrumental effects, such as pixel to pixel correlations or Poisson noise, or systematic effects (Banday et al. 2000). At the third decomposition scale (which is less affected by the instrumental effects), we detect a non-Gaussian signature with a probability $< 95\%$ in the southern hemisphere, whereas in the northern hemisphere, it is detected with a probability close to 99%. We have compared our results to those obtained by Mukherjee et al. (2000). Namely, we compare the results they obtain for what they note $k = 32$, 16 and 8, which correspond exactly to what we refer to as the diagonal details for respectively the first, second and third decomposition scales. We used the

**Table 5.** Probability for the excess of kurtosis of the COBE/DMR map (DSMB) to be attributed to a non-Gaussian signature. The numbers are given, for the three types of details, as a function of the decomposition scale and the wavelet basis. The first part of the table represents the north pole and the second part is for the south pole

| Wavelet basis | Scale | North pole | | | South pole | | |
|---|---|---|---|---|---|---|---|
| | | $\partial/\partial x$ | $\partial/\partial y$ | $\partial^2/\partial x\partial y$ | $\partial/\partial x$ | $\partial/\partial y$ | $\partial^2/\partial x\partial y$ |
| Haar | I | 66.3% | 99% | 58.9% | 64.1% | 81.5% | 86.5% |
| | II | 97.5% | 83.9% | 76.2% | 83.2% | 85.4% | 52.4% |
| | III | 57.5% | 71.9% | 79.9% | 79.5% | 73.4% | 43.6% |
| Villasenor et al. | I | 99.3% | 98.1% | 92.2% | 46.9% | 86% | 63% |
| | II | 81.8% | 50.8% | 77.7% | 98.4% | 92% | 65.4% |
| | III | 68% | 82% | 94.9% | 55.1% | 55.9% | 88.9% |

**Table 6.** Scale-scale correlation coefficients for the three types of details as a function of the wavelet basis. For the south and north pole, we give the probability for the correlation coefficient to be attributed to a non-Gaussian signal. The correlations are performed between the first and second scales, and between the second and third scales. The upper part of the table is given for the DSMB COBE/DMR maps whereas the lower part is for the DCMB maps

| Wavelet basis | Scale-scale | North pole | | | South pole | | |
|---|---|---|---|---|---|---|---|
| | | $\partial/\partial x$ | $\partial/\partial y$ | $\partial^2/\partial x\partial y$ | $\partial/\partial x$ | $\partial/\partial y$ | $\partial^2/\partial x\partial y$ |
| Haar | I–II | 65% | 75.5% | 70.9% | 79.8% | 60% | 86.1% |
| | II–III | 68.7% | 86.9% | 96.1% | 77.6% | 44% | 67.1% |
| Villasenor et al. | I–II | 99.3% | 70.1% | 86% | 63.4% | 95.2% | 80% |
| | II–III | 61.4% | 88.3% | 80.7% | 96.5% | 83% | 49.5% |
| Haar | I–II | 74.5% | 73.4% | 63.9% | 93.5% | 82.2% | 67.2% |
| | II–III | 83.8% | 93.9% | 96.4% | 86.6% | 72.3% | 68.1% |
| Villasenor et al. | I–II | 62.4% | 80.6% | 79% | 76.7% | 71.9% | 98% |
| | II–III | 73.5% | 80.2% | 81.2% | 83.3% | 71.5% | 57.3% |

dyadic decomposition advocated by Aghanim et al. (1998); Forni & Aghanim (1999); Aghanim & Forni (1999) rather than the pyramidal decomposition used in Hobson et al. (1999) and in Mukherjee et al. (2000). This choice is motivated by the fact that this particular decomposition scheme gives the correlations between the two directions of the map at each scale. It is not the case with the pyramidal decomposition which treats both directions as if they were independent. Another advantage of the dyadic decomposition is that, for each decomposition scale, the analysis bears upon the maximum number of coefficients possible. This is crucial for statistics in general and for the small COBE maps (#1 and 6) in particular.

The comparison between our results, obtained with the Villasenor et al. wavelet basis, and those of Mukherjee et al. (2000) shows that our non-gaussianity detection technique gives every time higher confidence levels except for two cases which are the first decomposition scale of the southern hemisphere (DCMB and DSMB maps). When we use the Haar wavelet basis, our confidence levels are higher than, or similar to, those quoted in Mukherjee et al. (2000) except for two cases that are the third decomposition scale of the northern and southern hemisphere of the DSMB map. Of course in addition to the diagonal details, we have two other criteria to detect the non-Gaussian signature (vertical and horizontal details). In particular, for the cases where the probability is smaller than in Mukherjee et al. (2000) we find a non-Gaussian signature based on the vertical or/and the horizontal details.

In our study, we find that the Villasenor et al. wavelet basis combined with a dyadic decomposition gives higher probabilities than the pyramidal decomposition. This basis is also more sensitive than the Haar basis. The better performances in detecting gradients come from the larger size of its kernel (Villasenor et al. 1995). However, this could become a weakness when a small number of pixels is available (small maps or high decomposition levels). In this case, the Haar wavelet basis could be more adapted due to the smaller size of its kernel.

Our choice of wavelet basis and decomposition scheme confirms that a non-Gaussian signature can be detected either in the south or the north galactic pole. It seems however that the statistical signature is less significant in the southern pole. In this case, the largest probability, $> 95\%$, is obtained only at the second decomposition scale for the DSMB COBE/DMR #6 map. The non-Gaussian signature is more significant for the north galactic pole as the probability is often $\geq 95\%$ and can even reach 99%. The scale-scale correlations represent a step further in the statistical analysis of the signal. However in our case,

it does not make a significant improvement in the results. The non-Gaussian signature is indeed detected with a probability of 99% at most, such as in the direct analysis.

The large size of the beam and pixels (respectively 7 and 2.8°) results in a rather small number of wavelet coefficients. This, together with the low signal to noise ratio of the COBE/DMR data, represent very limiting factors which prevent us from drawing any hasty conclusion from the rather marginal detections of the non-Gaussian signatures. This kind of statistical analyses will soon demonstrate all their performances when applied to the new generation of CMB data sets of higher sensitivity and resolution (Boomerang, De Bernardis et al. 2000 and Maxima, Hanany et al. 2000). We thus expect that these studies will then put constraints on the primordial non-Gaussian contributions such as the topological defects suggested for example in Bouchet et al. (2000).

*Acknowledgements.* This work is dedicated to the memory of our colleague Richard Gispert. We wish to thank G. Lagache for her help with the COBE data and E. Martinez-Gonzales for fruitful discussions. We also thank an anonymous referee for his helpful comments and suggestions.

## References

Aghanim, N., & Forni, O. 1999, A&A, 347, 409
Aghanim, N., Prunet, S., Forni, O., & Bouchet, F. R. 1998, A&A, 334, 409
Amendola, L. 1996, MNRAS, 283, 983
Banday, A. J., Zaroubi, S., & Gorski, K. M. 2000, ApJ, 533, 575
Bouchet, F. R., Peter, P., Riazuelo, A., & Sakellariadou, M. 2000 [astro-ph/0005022]
Bromley, B. C., & Tegmark, M. 1999, ApJ, 524, L79
De Bernardis, P., Ade, P. A. R., Bock, J. J., et al. 2000, Nat, 404, 955
Ferreira, P. G., Magueijo, J., & Gorski, K. M. 1998, ApJ, 503, L1
Fixsen, D. J., Cheng, E. S., Gales, J. M., et al. 1996, ApJ, 473, 576
Forni, O., & Aghanim, N. 1999, A&As, 137, 553
Hanany, S., Ade, P., Balbi, A., et al. 2000 [astro-ph/0005123]
Heavens, A. F. 1998, MNRAS, 299, 805
Hobson, M. P., Jones, A. W., & Lasenby, A. N. 1999, MNRAS, 309, 125
Kogut, A., Banday, A. J., Bennett, C. L., et al. 1996, ApJ, 464, L29
Magueijo, J. 2000, ApJ, 528, L57
Mallat, S. 1989, IEEE Trans. Patt. Anal. Machine Intell., 7, 674
Mukherjee, P., Hobson, M. P., & Lasenby, A. N. 2000 [astro-ph/0001385]
Pando, J., Lipa, P., Greiner, M., & Fang, L. Z. 1998a, ApJ, 496, 9
Pando, J., Valls-Gabaud, D., & Fang, L. Z. 1998b, Phys. Rev. Lett., 81, 4568
Schmalzing, J., & Gorski, K. M. 1998, MNRAS, 297, 355
Smoot, G. F., Bennett, C. L., Kogut, A., et al. 1992, ApJ, 396, L1
Villasenor, J. D., Belzer, B., & Liao, J. 1995, IEEE Trans. on Image Proc., 4, 1053